Reviewer Response

Reviewer C (Minor Comments)

Comment C1: "*Please check that all of the figures are referred to correctly, with the addition of new data some of the figure references are now incorrect*."

We have curated the manuscript to ensure that all figure callouts are accurately referenced in the manuscript.

Comment C2: "*For statistics it is stated that an ANOVA is used for all tests, even when there are only 2 groups. Please check if this is correct and edit appropriately*."

We have curated the manuscript to ensure that statistical analysis are accurately communicated in the figure legends.

Nuclear factor I-A regulates diverse reactive astrocyte responses after CNS injury

Dylan Laug[1,2*], Teng-Wei Huang[1*], Navish A Bosquez Huerta[1,2], Yu-Szu Huang[1,2], Debosmita Sardar[1], Joshua Ortiz[2,3], Jeffrey C Carlson[1,2], Benjamin R Arenkiel[2-5], Chay T Kuo[6], Carrie A Mohila[7], Stacey M Glasgow[8], Hyun Kyoung Lee [2-4,9], and Benjamin Deneen[1-4,10]

[1] Center for Cell and Gene Therapy, Baylor College of Medicine
[2] Program in Developmental Biology, Baylor College of Medicine
[3] Neurological Research Institute, Texas Children's Hospital
[4] Department of Neuroscience, Baylor College of Medicine
[5] Department of Human and Molecular Genetics, Baylor College of Medicine
[6] Department of Cell Biology, Duke University
[7] Department of Pathology, Texas Children's Hospital
[8] Department of Neurobiology, University of California San Diego
[9] Department of Pediatrics, Division of Neurology, Texas Children's Hospital
[10] Department of Neurosurgery, Baylor College of Medicine

Baylor College of Medicine
One Baylor Plaza
Houston, Tx. 77030

*Equal Contribution

Authors declare no conflicts of interest

Correspondence:

Benjamin Deneen
Center for Cell and Gene Therapy, Department of Neurosurgery
One Baylor Plaza, N1120.06
Houston, Tx 77030
Email: deneen@bcm.edu
Phone: 713-798-7897

Abstract

Reactive astrocytes are associated with every form of neurological injury. Despite their ubiquity, the molecular mechanisms controlling their production and diverse functions remain poorly defined. Because many features of astrocyte development are recapitulated in reactive astrocytes, we investigated the role of Nuclear Factor I-A (NFIA), a key transcriptional regulator of astrocyte development whose contributions to reactive astrocytes remains undefined. Here we show that NFIA is highly expressed in reactive astrocytes in human neurological injury and identify unique roles across distinct injury states and regions of the CNS. In the spinal cord, after white matter injury (WMI) NFIA-deficient astrocytes exhibit defects in blood-brain-barrier remodeling, which is correlated with the suppression of timely remyelination. In the cortex, after ischemic stroke, NFIA is required for the production of reactive astrocytes from the sub-ventricular zone (SVZ). Mechanistically, NFIA directly regulates the expression of Thrombospondin4 (Thbs4) in the SVZ, revealing a key transcriptional node regulating reactive astrogenesis. Together, these studies uncover critical roles for NFIA in reactive astrocytes and illustrate how regional- and injury- specific factors dictate the spectrum of reactive astrocyte responses.

Introduction

Reactive astrocytes are associated with most forms of neurological disorder, ranging from acute injury to degeneration (1) and exhibit diverse roles in these disease states. They are generally viewed as beneficial during acute injury response and deleterious during chronic, or later stages of recovery (2-7). These paradigms were initially established in spinal cord injury models, however recent studies on astrocyte diversity have illustrated immense regional and local diversity in the adult brain suggesting that these disparate roles may be the result of a vast reservoir of reactive astrocyte populations (4,8). When this cellular and regional complexity is met with the wide spectrum of disease states that elicit reactive astrocyte responses (7), a complex interplay between diverse resident astrocytes and disease-specific factors emerges. Therefore, deciphering how diverse reactive astrocyte responses are regulated is critical for understanding their contributions to neurological disease.

Despite their ubiquity, the molecular processes that oversee the production of reactive astrocytes after injury remain poorly defined. Critically, reactive astrocytes display a number of features that call to mind their developmental origins, including GFAP upregulation, increased proliferative capacity, and hypertrophy (9,10). While these are generic features of all reactive astrocytes, using them as molecular entry points and drawing connections to their developmental origins can provide valuable insight into their diverse, post-injury functions (11). For example, STAT3 plays a key role in the generation of astrocytes during development and several, diverse roles in reactive astrocytes. Conditional deletion of STAT3 in astrocytes impairs glial scar formation after spinal cord injury (SCI), indicating a role in their proliferation or migration

132 (12). Separately, in white matter injury (WMI) models, conditional deletion of STAT3
133 suppressed remyelination via cell non-autonomous mechanisms through promotion of
134 TGFβ-1 expression in microglia (13). These observations highlight the critical
135 contributions of factors that regulate astrocyte development to reactive astrocyte
136 responses after injury. Moreover, they point to their diverse roles across a host of
137 neurological disease states, suggesting that developmental factors may be a key to
138 understanding the underlying functional diversity of reactive astrocytes.

139 Nuclear Factor I-A (NFIA) is a transcription factor that plays a central role in
140 astrocyte development, where it is required for the initiation of gliogenesis and
141 differentiation of astrocytes by directly regulating key genes essential for astrocyte
142 identity (14,15). Additionally, we found that NFIA plays a key role in several neurological
143 diseases including glioma and WMI (16-18). Studies on NFIA in WMI focused on its
144 expression in oligodendrocyte precursor populations, finding that its ectopic expression
145 is sufficient to suppress remyelination (18). However, whether it is necessary for
146 remyelination and the cellular origins of this function remain undefined. Critically, while
147 NFIA is transiently expressed in oligodendrocyte precursors, it continues to be
148 expressed in mature astrocytes, in the adult brain (14-16,18). These observations,
149 coupled with its essential role in astrocyte development, suggest that NFIA may
150 contribute to CNS injury responses through reactive astrocytes; currently, whether and
151 how NFIA regulates reactive astrocyte responses after CNS injury is unknown.

152 To initiate studies on NFIA in reactive astrocytes, we evaluated its expression in
153 human adult WMI and neonatal ischemic stroke, finding that it is highly expressed in
154 reactive astrocytes in both of these injury states. Combining conditional mouse genetics

155 with spinal cord WMI models and cortical ischemic stroke models, we found that NFIA
156 plays region- and injury-specific roles in reactive astrocytes. In the spinal cord, after
157 WMI, NFIA-deficient astrocytes exhibit defects in blood-brain-barrier remodeling, which
158 is correlated with the suppression of timely remyelination. In the cortex, after ischemic
159 stroke, NFIA is required for the production of reactive astrocytes from the sub-
160 ventricular zone (SVZ). Mechanistically, NFIA directly regulates the expression of
161 Thbs4 in the SVZ, illustrating a key transcriptional node that oversees reactive
162 astrogenesis after stroke. Together, these studies represent the initial characterization
163 of NFIA function in reactive astrocytes after injury and show that it executes distinct
164 functions that are both region- and injury- dependent. Taken more broadly, these
165 diverse functions of a single transcription factor reinforce the importance of decoding
166 the complex cellular and injury interplay that dictates the spectrum of reactive astrocyte
167 responses.
168
169 **Results**
170 *NFIA is expressed in reactive astrocytes in human WMI*
171 Our previous studies on NFIA demonstrated its expression in oligodendrocyte precursor
172 (OLPs) populations that occupy human multiple sclerosis (MS) and hypoxic-ischemic
173 encephalopathy (HIE) lesions (18). To determine whether NFIA is also expressed in
174 reactive astrocytes present in lesions found in these diseases, we performed double
175 immunofluorescence staining for NFIA and GFAP, a defining marker of reactive
176 astrocytes (1). Using paraffin-embedded human brain tissue obtained from the Rocky
177 Mountain MS Center at University of Colorado (MS lesion) and Texas Children's

178 Hospital (HIE lesions), we found that NFIA is highly expressed in reactive astrocytes
179 occupying these lesions (**Fig.1A-F**). While NFIA demonstrated robust expression in
180 reactive astrocytes, not every GFAP-expressing cell exhibited NFIA expression,
181 suggesting that its expression may be restricted to subsets of reactive astrocyte
182 populations. Moreover, consistent with its expression in OLP populations, NFIA
183 expression is also not limited to GFAP-expressing populations.
184 To initiate injury modeling studies, we first evaluated NFIA expression in reactive
185 astrocyte populations found in two mouse injury models that parallel the human disease
186 states described above. To model remyelination after WMI we used lysolecithin
187 lesioning of the spinal cord and to model ischemic stroke, we used cortical
188 photothrombotic stroke (19,20) (**Supplemental Figure S1**). Critically, both models
189 produce a robust reactive astrocyte response and using double immunofluorescence,
190 we found that NFIA co-localizes with GFAP-expressing reactive astrocytes in these
191 models (**Fig.1G-L**). Subsequent analysis of normal, non-reactive astrocytes in
192 uninjured regions of the human and mouse cortex, revealed that NFIA is also expressed
193 in resident astrocytes in the healthy brain, suggesting that it's expression is not an
194 injury-specific phenomenon (**Supplemental Figure S2**). Together these data from
195 primary human samples and relevant animal models indicate that NFIA is expressed in
196 reactive astrocytes associated with WMI and ischemia.
197
198 *Loss of NFIA in astrocytes delays remyelination after WMI in the spinal cord*
199 To examine whether NFIA contributes to disease pathogenesis through a prospective
200 function in reactive astrocytes, we generated floxed-NFIA alleles and intercrossed this

201 line with GFAP-CreER or Sox10-Cre, generating the following lines: *NFIA$^{fl/fl}$; GFAP-*
202 *CreER* and *NFIA$^{fl/fl}$; Sox10-Cre.* These lines allow us to selectively delete NFIA in either
203 OLP populations (Sox10-Cre) or adult astrocyte populations (GFAP-CreER), offering
204 the opportunity to resolve its cellular site of action. To determine the role of NFIA in
205 remyelination after WMI, we performed lysolecithin lesioning in the spinal cord of these
206 mouse lines, evaluating the cellular responses 10 days post-lesioning (10dpl), a critical
207 timepoint that corresponds with the commencement of remyelination in the spinal cord
208 (21,22). As shown in figure 2A-J, deletion of NFIA in OLPs (i.e. *NFIA$^{fl/fl}$; Sox10-Cre*)
209 does not influence the generation of OLPs, GFAP-expressing reactive astrocytes, nor
210 have any effect on the kinetics of OLP differentiation into oligodendrocytes during
211 remyelination. These data indicate that loss of NFIA in OLPs does not influence
212 remyelination after WMI.
213 To determine whether NFIA functions through astrocytes, we performed
214 lysolecithin lesioning on *NFIA$^{fl/fl}$; GFAP-CreER* mice. Use of the tamoxifen inducible
215 GFAP-CreER allows us to bypass any developmental requirements for NFIA in
216 astrocytes or their precursors, enabling us to focus on adult astrocyte populations post-
217 injury. As shown in figure 2K, we treated mice with tamoxifen starting at six weeks of
218 age, then performed lysolecithin lesioning three weeks later. Analysis of the cellular
219 responses during early remyelination (i.e. 10dpl), revealed efficient deletion of NFIA
220 (**Fig.2L, P**), coupled with no overt changes in the number of OLPs marked by Olig2 or
221 reactive astrocytes, marked by GFAP (**Fig.2M-N v. Q-R; U-V**). Next, we evaluated the
222 extent of oligodendrocyte differentiation and found a significant decrease in number of
223 PLP- and MBP-expressing cells within the lesions of *NFIA$^{fl/fl}$; GFAP-CreER* mice

224 (**Fig.2O,S, T; Supplemental Figure S3**). Importantly, these changes in oligodendrocyte
225 differentiation are not secondary to axonal loss, as axonal integrity is not differentially
226 affected after injury in these mouse lines (**Supplemental Figure S3**). Subsequent
227 analysis at 12dpl (two days later) revealed that lesions in the *NFIA$^{fl/fl}$; GFAP-CreER*
228 mice contained PLP- and MBP- expressing cells, indicating a delay in the onset of OLP
229 differentiation (**Supplemental Figure S3**). Together, these data indicate that loss of
230 NFIA in astrocytes does not influence the generation of OLPs or reactive astrocytes, but
231 rather influences the kinetics of oligodendrocyte differentiation after WMI in the spinal
232 cord.
233
234 *NFIA-deficient reactive astrocytes demonstrate defective BBB after WMI*
235 These effects on oligodendrocyte differentiation via NFIA-deletion in astrocytes are
236 likely to be mediated via cell non-autonomous mechanisms. Given that reactive
237 astrocytes are still present in these lesions, we hypothesized that reactive astrocyte
238 function in the absence of NFIA was impaired. One key function of reactive astrocytes is
239 to reestablish the blood-brain-barrier (BBB) after injury, moreover it's been previously
240 shown that impaired BBB can suppress oligodendrocyte differentiation after WMI (23).
241 To determine whether the BBB is impaired in *NFIA$^{fl/fl}$; GFAP-CreER* lesions, we stained
242 for proteins associated blood proteins associated with BBB leakage (albumin), finding
243 very high levels in lesions from *NFIA$^{fl/fl}$; GFAP-CreER* mice (**Fig.3A v. C, E**). This
244 suggests impaired BBB remodeling after WMI. Given the role of astrocyte endfeet
245 proteins in establishing the BBB (24), we evaluated the expression of Aqp4, finding its
246 expression is also reduced in the absence of NFIA (**Fig.3B v. D, F**). To determine

247 whether these defects in BBB integrity are specific to injury conditions or a general
248 feature of this mouse line, we performed the Evans blue assay on uninjured *NFIA*$^{fl/fl}$*;*
249 *GFAP-CreER* and control mice, finding no differences in the amount of Evans blue
250 extracted from both the spinal cord and cortex of these mice (**Supplemental Figure**
251 **S5**). Together, these data suggest that the impaired BBB observed in the presence of
252 NFIA-deficient astrocytes is an injury-specific phenomenon.
253 To directly examine whether astrocytes lacking NFIA influence the formation of
254 tight junctions between endothelial cells, we performed co-culture assays and evaluated
255 the trans-endothelial electrical resistance (TEER) across this bilayer, an established
256 metric of endothelial integrity (25). Towards this, we established astrocyte cultures from
257 *NFIA*$^{fl/fl}$*; GFAP-CreER* mice and added tamoxifen to induce deletion of NFIA; two weeks
258 after tamoxifen induced deletion of NFIA we co-cultured these astrocytes with brain
259 endothelial cells (bEnd3) (**Fig.3G**). Upon establishing the co-culture, we measured
260 TEER across this cell bilayer to assay the extent of ion passage across the tight
261 junctions that form between endothelial cells, finding decreased electrical resistance
262 across this cell bilayer in the presence of NFIA-deficient astrocytes (**Fig.3H**). This
263 decrease in TEER indicates that fewer tight junctions were formed between endothelial
264 cells in the presence of NFIA-deficient astrocytes. These data, in conjunction with our
265 analysis of the lesions, indicate that loss of NFIA in reactive astrocytes results in
266 impaired BBB integrity after WMI in the spinal cord.
267
268
269

270 *NFIA is required for the production of reactive astrocytes after cortical ischemic stroke*

271 The forgoing results implicate NFIA as a key mediator of BBB remodeling in reactive
272 astrocytes after WMI. To further evaluate this function of NFIA in reactive astrocytes, we
273 extended our studies to the photothrombotic model of cortical ischemia where
274 thrombosis results in disruption of endothelial cell integrity (**Supplemental Figure S1**).
275 Critically, NFIA is also highly expressed in reactive astrocytes in this model and in
276 human ischemic disease states (**Fig.1**), providing further rationale for these studies.
277 Similar to our WMI studies, we used the *NFIA$^{fl/fl}$; GFAP-CreER* mice (and *NFIA$^{fl/+}$;*
278 *GFAP-CreER* controls) and a defined tamoxifen schedule that allowed us to delete
279 NFIA prior to photothrombotic stroke injury (**Fig.4A**). Analysis of cellular outcomes
280 twelve days post-injury revealed efficient deletion of NFIA at the stroke site (**Fig.4C,F**),
281 coupled with a dramatic reduction in the number of GFAP-expressing reactive
282 astrocytes (**Fig.4B v. E, N**). This reduction in GFAP-positive reactive astrocytes
283 occurred at the injury border and adjacent to the injury site (**Fig.4H,K**). Furthermore, we
284 observed increased presence of blood proteins (albumin) at the injury site (**Fig.4D v. G**)
285 which is consistent with the reduced production of reactive astrocytes and the
286 associated impaired injury response. These observations suggest a depletion of
287 resident astrocytes or an inability of resident astrocytes to acquire reactive properties.
288 To decipher between these possibilities, we stained the injury border and adjacent
289 regions with Sox9, an established maker of mature astrocytes in the brain (26). As
290 shown in figure 4O, there is no change in the number of Sox9-expressing cells at the
291 injury site, nor in adjacent regions, indicating that loss of NFIA is not influencing the
292 survival or local proliferation of astrocytes in the cortex after ischemic stroke injury.

293 Together, these data suggest that NFIA expression is necessary for local astrocytes to
294 acquire reactive properties after ischemic stroke in cortex and together with our spinal
295 cord WMI studies, suggest that it has region and/or injury specific functions in reactive
296 astrocytes.

297 To ascertain whether NFIA demonstrates region specific functions in reactive
298 astrocytes, we performed lysolecithin lesioning in the corpus callosum of the adult brain,
299 using the *NFIA$^{fl/fl}$; GFAP-CreER* mouse lines and the tamoxifen induction paradigm
300 shown in Figure 2K. Oligodendrocyte regeneration was evaluated 12 days-post-
301 lesioning of the corpus callosum, a relatively early timepoint in the myelin repair process
302 for this region (27). Our analysis revealed no changes in the extent of oligodendrocyte
303 differentiation or in the production of reactive astrocytes in these lesions (**Supplemental**
304 **Figure S4**), indicating that loss of NFIA does not influence repair in this context. These
305 data, in conjunction with our spinal cord studies and ischemic stroke studies, indicate
306 that the role of NFIA in reactive astrocyte responses varies across both injury-type and
307 region of the CNS.

308

309 *Reactive astrogenesis in the SVZ is impaired in the absence of NFIA*

310 To understand the cellular mechanism by which NFIA controls the generation of
311 reactive astrocytes after cortical ischemia, we focused on reactive astrogenesis from the
312 sub-ventricular zone (SVZ). Previous studies have shown that the SVZ is a source of
313 reactive astrocytes that emigrate to injury sites after cortical ischemia, and that a loss of
314 SVZ-derived reactive astrocytes dramatically impairs injury response and recovery
315 (19,28). To determine whether SVZ responses after ischemic injury are also affected by

316 loss of NFIA, we implemented our deletion/injury paradigm (**Fig.4A**), treated with BrdU
317 at five days post-injury, and subsequently harvested cortices from *NFIA$^{fl/fl}$; GFAP-*
318 *CreER* or control mice. First, we found that NFIA is highly expressed in BrdU-positive
319 cells occupying the SVZ under these conditions in control animals (**Fig.5A-C**), indicating
320 that it is expressed in cell populations that are able to generate reactive astrocytes.
321 Next, we evaluated BrdU-incorporation in the SVZ in the absence of NFIA, finding an
322 efficient deletion of NFIA in this region (**Fig.5A v. D**), coupled with a drastic decrease in
323 the extent of cellular proliferation (**Fig.5B v. E**). Interestingly, decreased BrdU-
324 incorporation within the SVZ in the *NFIA$^{fl/fl}$; GFAP-CreER* mice was also observed
325 under non-injury conditions (**Supplemental Figure S5**), indicating that NFIA plays a
326 general role in maintaining proliferative populations in the SVZ under homeostatic
327 conditions. These data indicate that NFIA is required for SVZ proliferation in the
328 uninjured brain and after cortical ischemia, suggesting that defects in reactive
329 astrogenesis could be a result of these defects in the SVZ.
330 The forgoing data implicate the SVZ as one of NFIA's prospective sites of action
331 in this post-injury context. To test whether defects in reactive astrogenesis are due to
332 loss of NFIA in the SVZ, we employed viral mediated approaches to selectively delete it
333 in the SVZ. Towards this, we generated *NFIA$^{fl/fl}$; Rosa-flox-tdTomato* mouse lines and
334 injected the SVZ of these mice with Ad5 virus containing Cre (**Fig.5H**). This approach
335 enabled the following: i) fate mapping Ad5-Cre infected cells in the SVZ after injury and
336 ii) specific deletion of NFIA from SVZ populations. Following the injection/injury
337 paradigm depicted in figure 5H, we found a host of tdTomato-labeled, NFIA-expressing
338 cells at the injury site, that also co-expressed GFAP in control animals (**Fig.5I-L**). These

339 observations indicate that a subset of reactive astrocytes at the ischemic injury site are
340 derived from NFIA-expressing cells from the SVZ. Next, we performed the same
341 experiment in the *NFIA$^{fl/fl}$; Rosa-flox-tdTomato* mouse and found a drastic decrease in
342 the number of tdTomato-labeled cells co-expressing NFIA at the injury site (**Fig.5M-N,**
343 **Q**), as well as a decrease in the number of GFAP-expressing reactive astrocytes
344 (**Fig.5O-P**). Critically, analysis of the SVZ of these mice revealed that a majority of the
345 tdTomato-labeled cells remained in the SVZ, indicating that the cells infected with Ad5-
346 Cre remained in the SVZ and did not mount an injury response (**Supplemental Figure**
347 **S5**). These data, in conjunction with our analysis of the post-injury SVZ, indicate that
348 NFIA is required for SVZ-astrogenesis after ischemic injury.
349
350 *NFIA directly regulates Thbs4 expression*
351 Next, we sought to decipher the mechanism by which NFIA regulates post-ischemic
352 SVZ-astrogenesis. Previous studies have shown that Thrombospondin4 (Thbs4) is
353 required for SVZ-astrogenesis after photothrombotic stroke (19) and our results show
354 that conditional NFIA knockout in astrocytes phenocopies the Thbs4 knockout, which
355 suggests a link between these genes. Because NFIA is a transcription factor and Thbs4
356 is expressed in the SVZ and immediately adjacent regions (19), we hypothesized that
357 Thbs4 may be a target of NFIA. To investigate this possibility, we first evaluated Thbs4
358 expression in NFIA-deficient mice, finding that its expression is completely eliminated in
359 the SVZ, rostral migratory stream (RMS), and corpus callosum (CC) in the absence of
360 NFIA in the normal brain and after ischemic injury (**Fig.6A-E; Supplemental Figure**
361 **S6**). Next, we queried the core promoter region of Thbs4, identifying a prospective NFIA

362 binding site proximal to the transcriptional start site, that we confirmed via chromatin
363 immunoprecipitation (ChIP) with NFIA antibodies on cultured astrocytes (**Fig.6F-G**).
364 Finally, we cloned the core promoter of Thbs4 that contains this NFIA binding site and
365 found that increasing concentrations of NFIA can effectively activate this promoter
366 region (**Fig.6H**). Together, these genetic and biochemical data indicate that Thbs4 is a
367 direct transcriptional target of NFIA in the SVZ.

368 Our collective studies suggest a model by which NFIA regulates Thbs4
369 expression in the SVZ after ischemic stroke and that this transcriptional node plays a
370 critical role in reactive astrogenesis. To evaluate whether this relationship exists in
371 human ischemic injury, we performed double immunolabeling with NFIA and Thbs4 in
372 human HIE samples. As shown in figure 6I-K, NFIA and Thbs4 are highly co-expressed
373 in subsets of cell populations present in human HIE samples. These data provide
374 validation for our mouse studies and are evidence that this regulatory node is present in
375 human reactive astrocytes.
376

377 **Discussion**

378 These studies identify NFIA, a transcription factor that is crucial to glial development, as
379 a novel regulator of reactive astrocyte generation and function within diverse models of
380 white matter disease and ischemia. Using lineage-specific loss of function approaches,
381 we identified NFIA as critical transcriptional regulator in astrocytes during BBB
382 remodeling after WMI in the spinal cord and reactive astrocyte generation following
383 ischemic events in the cortex. In addition, we identified NFIA as a key regulator of SVZ-

384 mediated reactive astrocyte response to cortical ischemia injuries via direct
385 transcriptional control of Thbs4.
386
387 *NFIA plays a critical role in reactive astrocyte responses during injury*
388 In this study, we show that NFIA is expressed within reactive astrocytes present in adult
389 MS and neonatal HIE lesion tissue and representative mouse models of such disorders.
390 Moreover, when NFIA is specifically deleted from the astrocyte lineage, the functional
391 response of reactive astrocytes in two different CNS injury models is impaired.
392 Ultimately, these impairments results in delayed remyelination within spinal cord WMI
393 models and persistent presence of blood serum proteins in an ischemic stroke model.
394 Together, this data suggests that NFIA is a critical transcriptional regulator of reactive
395 astrocyte responses to CNS insult and highlights several novel roles for NFIA in specific
396 aspects of reactive astrocyte function, including their production from the SVZ and
397 maintenance of the BBB after injury.
398 These findings highlight critical parallels between glial development and glial
399 response after injury. During development, NFIA expression within neural precursor
400 cells of the spinal cord is necessary and sufficient to initiate gliogenesis (14,15). Our
401 data suggests that NFIA is similarly important for the generation of reactive
402 astrogenesis within the SVZ after a cortical ischemic injury. Interestingly, other factors
403 important to glial development have also been linked to reactive astrocyte responses to
404 injury. A number of studies have implicated the JAK-STAT pathway as important to glial
405 development through the inhibition of pro-neural transcription factors and induction of
406 glial genes via the JAK-STAT mediator STAT3 (29-32). Similar to the developmental

407 parallels highlighted in our study of NFIA, studies utilizing spinal cord injury models
408 found that the loss of STAT3 impairs reactive astrocyte responses and results in
409 aberrant reactive astrocyte function after injury (12,13). Other examples include the
410 requirement of Notch signaling receptor Notch1 in both cerebellar glial development and
411 in the generation of reactive astrocytes in response to stroke events (33,34). Moreover,
412 Notch-signaling in reactive astrocytes can suppress OLP repair after WMI
413 (35).Together, these studies mirror and complement our findings regarding the
414 importance of key regulators of glial development in reactive astrocyte generation and
415 function after CNS insult.
416 In future studies, it will be important to understand how these developmental
417 factors cooperate in the regulation of reactive astrocyte generation and function.
418 Considering Stat3 and NFIA have been shown to cooperate in the transcriptional
419 regulation of GFAP expression during developmental gliogenesis (36), there is a
420 possibility that such relationships persist post-development, especially in the context of
421 reactive gliosis. Similar mechanistic relationships between NFIA and the omnipotent
422 Notch-signaling pathway may also reveal critical developmental processes that are
423 repurposed after injury.
424
425 *Regional- and injury-specific roles for NFIA in reactive astrocytes*
426 By subjecting NFIA conditional mutants to WMI within the spinal cord and corpus
427 callosum, and ischemia within the cortex, we have demonstrated that it has distinct
428 functions within astrocyte populations in these different contexts. Among reactive
429 astrocytes of the spinal cord, NFIA is vital for the integrity of the BBB after WMI, but not

430 in the corpus callosum in the adult brain. These data suggest that NFIA is playing a
431 region-specific role in reactive astrocyte responses to WMI, highlighting an underlying
432 functional diversity across these regions. These observations are in stark contrast to our
433 findings in models of cortical ischemia, where NFIA is crucial for both the production of
434 reactive astrocytes via proliferation within the SVZ and the acquisition of reactive
435 characteristics. Collectively, these observed differences in the function of NFIA in
436 reactive astrocytes within the spinal cord versus the cortex, across distinct injury
437 paradigms, provides an important conceptual advance – a single transcription factor can
438 execute regionally and/or injury specific functions within the same lineage.

439 This raises the possibility that there are injury- and/or region-specific factors that
440 influence how NFIA operates in reactive astrocytes in order to modulate their generation
441 and function. Because different types of CNS injuries and diseases result in varying
442 amounts of cell death, inflammation, cellular responses, and tissue replacement and
443 remodeling, it is possible that these events result in differential signaling and release of
444 factors within the injury parenchyma that coordinate cellular responses unique to a
445 specific CNS insult (37). Indeed, a number of studies have begun to characterize the
446 molecular response of reactive astrocytes to different signaling events that occur as a
447 result of injury (38-40).

448 Also, when considering diverse reactive astrocyte response, one must be mindful
449 of regional diversity. Recent studies have shown that different brain regions harbor
450 diverse populations of astrocytes that exhibit both molecular and functional differences
451 (8,41,42). While the source of this diversity remains largely unknown, it's possible that
452 brain anatomy and the underlying proximity and relationship of astrocytes to other CNS

453 cells and structures is at least partially responsible. In support of this, one study has
454 shown that postnatal astrocytes of the dorsal spinal cord differ significantly in their gene
455 expression profiles from their ventral counterparts (43). Are similar positional cues
456 giving rise to the functional diversity of NFIA in reactive astrocytes and could these
457 same positional cues also drive diverse functions for NFIA in non-reactive astrocytes? If
458 such regionality exists, it calls to mind patterning mechanisms underlying nervous
459 system development in which the positional cues direct the differentiation of progenitors
460 into distinct cell population (44,45). Thus, understanding how patterning mechanisms
461 contribute to astrocyte responses, is yet another area of development that may
462 influence CNS injury and associated responses (46). Critically, a detailed understanding
463 of regional diversity of reactive astrocytes, as well as how different injury types influence
464 these diverse reactive astrocytes, may lead to more selective therapies that aid in
465 stimulating specific repair programs leading to better patient outcomes.
466
467 *Transcriptional control of injury-induced SVZ-astrogenesis*
468 Our studies also describe a novel transcriptional link between NFIA and Thbs4 in the
469 SVZ that regulates the generation of reactive astrocytes in response to a cortical
470 ischemic event. Thbs4 has previously been identified as a key regulator of the SVZ
471 reactive astrocyte response (19). Our studies have shown that the loss of NFIA results
472 in a significant decrease in the expression of Thbs4 within the SVZ (Fig. 6). Coupled
473 with our findings that NFIA directly regulates Thbs4 expression and that its loss from the
474 SVZ phenocopies the reduced reactive astrocyte response in Thbs4 KO mice, suggest
475 that NFIA's regulation of Thbs4 is an important mediator of the SVZ cellular response to

476 cortical ischemia. Together, this reveals a novel role for NFIA in the generation of RAs
477 from the SVZ after such cortical injuries.
478 This data raises the possibility that NFIA may also be involved in the
479 transcriptional control of reactive astrocyte responses from the SVZ in other diseases
480 and injuries. Previous studies have found that the SVZ can generate oligodendrocytes
481 in response to white matter damage within the corpus callosum and periventricular
482 white matter and EGFR signaling within the SVZ is important for this response (47-49).
483 These observations, coupled with our data showing that NFIA regulates the proliferation
484 and subsequent generation of reactive astrocyte responses from these same SVZ
485 progenitor populations after injury, raise interesting questions about the role that NFIA
486 may play in mounting a SVZ proliferative response to any number of injuries within the
487 brain. These dividing cells may then be influenced by injury-specific signaling events,
488 such as EGFR signaling, to generate different proportions of reactive astrocytes or
489 OLPs as required for the repair of that specific injury. More broadly, NFIA has been
490 shown to directly repress the cell cycle regulator p21 in a mouse neural stem cell model
491 of glioma, suggesting NFIA may have roles in promoting proliferation outside of the SVZ
492 after injury (50). Several studies have shown that reactive astrocytes exhibit some
493 localized proliferative capacity at CNS injury sites (34,51). Because NFIA is expressed
494 by reactive astrocytes, it is possible that NFIA plays a role in the proliferation that occurs
495 at the injury periphery among these cells.
496 Our data has identified NFIA as a central regulator of SVZ reactive astrocyte
497 production after cortical ischemia through direct transcriptional activation of Thbs4.
498 Thbs4 has been shown to physically interact with Notch1 to activate downstream

499 effectors of the Notch pathway. Interestingly, these studies found that NFIA expression
500 increased in primary SVZ-derived neural stem cells after being treated with Thbs4 (19).
501 However, they found no significant decrease in NFIA expression in Thbs4 KO animals
502 (19). In conjunction with our data regarding NFIA's direct transcriptional regulation of
503 Thbs4, this suggests that there may be positive feedback activation of NFIA through its
504 activation of Thbs4 transcription. Intriguingly, our data provides genetic evidence that
505 Thbs4 expression is dependent on NFIA in homeostatic, non-injured conditions,
506 suggesting that NFIA operates primarily upstream of Thbs4. Because these previous
507 studies of the relationship of Thbs4 to Notch and NFIA primarily focused on injury
508 conditions, it is possible that this positive feedback loop only occurs within the SVZ in
509 response to injury states. If true, this is would support the hypothesis that NFIA exhibits
510 functional diversity in gene regulation when the CNS is subjected to injury.
511

512 **Methods**

513 *Genetic knock-out of NFIA*

514 *NFIA*$^{fl/fl}$ conditional mutant mice were generated using targeted mutation of embryonic
515 stem (ES) cells from the European Mouse Mutant Cell Repository (EUMMCR Clone ID:
516 HEPD0646_5_E04). ES cells were injected into 3.5 days post coitum (dpc) blastocysts
517 which were then transferred into pseudo-pregnant mothers, all according to protocols
518 available on the EUMMCR website. *NFIA*$^{fl/+}$ mice were then intercrossed to generate
519 *NFIA*$^{fl/fl}$ animals.

520 Targeted knockout of NFIA was regulated with the following mouse lines: GFAP-
521 CreERT2 (Jackson Labs, stock no. 012849 and Sox10-Cre (Gift from Dr. Jeff Neul,

522 Vanderbilt University). All housing and breeding procedures were approved by the
523 Institutional Animal Care and Use Committee at Baylor College of Medicine and
524 conform to the US Public Health Service Policy on Human Care and Use of Laboratory
525 Animals.

526 To induce recombination in the GFAP-CreERT2 mouse line, animals were
527 injected intraperitoneally 1x daily for 5 consecutive days with a 100 mg/kg body weight
528 of Tamoxifen (Sigma-Aldrich) (dissolved 10 mg/mL in a 9:1 corn oil/ethanol mixture).
529 This regiment was sufficient to induce recombination in greater than 95% of GFAP+
530 cells surveyed by NFIA and GFAP immunofluorescence for the GFAP-CreERT2 line.
531

532 *In situ hybridization and immunohistochemistry*

533 mRNA in situ hybridization probes generated for mouse myelin proteolipid protein (PLP)
534 were generated and *in situ* hybridization (ISH) protocol was performed as previously
535 described[4]. mRNA probe for mouse thrombospondin4 (Thbs4) was generated using
536 primers obtained from the Allen Brain Atlas (Forward primer:
537 AGGGAGCAGAAGAGTCACCAT, Reverse primer: GACTGAAAGCTGAGAGGACCAC)
538 according to previously published methods (52). Double ISH/immunohistochemistry was
539 performed as previously described (14). Briefly, fluorescent ISH for Thbs4 on human
540 hypoxic ischemic encephalopathy tissue was performed first and developed with α-
541 Digoxigenin-POD (Roche) and then fluorescently amplified using TSA Plus Cy5
542 Fluorescence System (PerkinElmer). Following ISH, fluorescence staining for NFIA was
543 performed using rabbit anti-NFIA (Sigma-Aldrich, 1:500) as described below.

544 For immunohistochemistry analysis of this tissue, slides with sections were
545 washed in 1x PBS 3 times, blocked for 1 hour in 5% goat serum in PBS with 0.01%
546 Triton added (excluded from blocking solution used for membrane bound proteins),
547 followed by incubation with primary antibody dilutions overnight. Primary antibodies
548 were used at the following concentrations: rabbit anti-Olig2 (AB9610, Abcam, 1:1,000),
549 rabbit anti-GFAP (Z0334, Dako, 1:1,000), mouse anti-GFAP (MAB360, Millipore, 1:500),
550 rabbit anti-NFIA (HPA006111, Sigma-Aldrich, 1:500), rabbit α-Sox9 (Ab5535, Millipore,
551 1:1000), , rabbit anti-Albumin (ab135575, Abcam, 1:100), rabbit anti- Aquaporin 4
552 (AB2218, Millipore, 1:250), rat anti-BrdU (ab6326, Abcam, 1:500), mouse anti-Cre
553 (MAB3120, Millipore, 1:500), chicken anti-neurofilament heavy polypeptide (ab4680,
554 Abcam, 1:1000), mouse anti-nonphosphorylated neurofilament H(801702, BioLegend,
555 1:800), and goat anti-Thrombospondin 4 (sc-390734, Santa Cruz Biotechnology, 1:150).
556
557 *Lysolecithin-induced demyelination model*
558 Demyelinated lesions were generated in the ventrolateral white matter of the spinal cord
559 or the corpus callosum of 8-10-week-old mice as previously described (11,16). Briefly,
560 the ventral white matter of the spinal cord was injected with 0.5 uL of 1% lysolecithin
561 (Sigma-Aldrich) dissolved in sterile 1x PBS solution using a 10 uL Hamilton syringe and
562 KD Scientific syringe pump system. Mice were harvested at 10dpl and were trans-
563 cardially perfused with ice cold 1x sterile PBS followed by a 30mL perfusion of 4%
564 paraformaldehyde at a rate of 1 mL/minute using a Fisher-Scientific variable speed
565 mini-pump. CNS tissues were then dissected and fixed in 4% paraformaldehyde
566 overnight and then cryo-protected in 30% sucrose an additional 24 hours. Tissue

567 samples were then frozen in Tissue-Tek Optimal Cutting Temperature compound
568 embedding medium and sectioned in 20 micron sections directly mounted to glass
569 slides. All animal procedures were done in accordance with approved BCM IACUC
570 protocols.
571
572 *Photothrombotic focal ischemia model*
573 Focal ischemic sites were generated in the cortex of 8-10-week-old mice using methods
574 previously described[20]. Briefly, mice were injected intraperitoneally with 10 ul/g body
575 weight Rose Bengal dye dissolved (15 mg/ml) in sterile phosphate buffered saline. After
576 waiting 15 minutes for the dye to enter and circulate via the blood stream, the mouse is
577 anesthetized using isoflurane (2% in 2 L/min oxygen) and an incision was made in the
578 skin overlaying the skull. Next, a Leica KL 300 LED light affixed with a custom-made 1
579 mm diameter aperture is centered at 0.5 mm anterior and 1.0 mm lateral to Bregma.
580 The underlying vasculature is exposed to light via this source for 15 minutes, upon
581 which the light is turned off, the skin is sutured, and the animal is allowed to recover in
582 sternal recumbency until fully awake. Upon harvest at 12 or 14 days post injury (dpi),
583 animals were perfused and tissue was processed as described above. All animal
584 procedures were done in accordance with approved BCM IACUC protocols.
585
586 *Cre-virus injection in SVZ*
587 For all stereotaxic injections, mice were anesthetized using vaporized isoflurane and
588 were maintained under anaesthesia using 2% isofluorane O2. All injections were
589 performed using a stereotaxic apparatus synced to Angle Two software for coordinate

590 guidance. For Cre-virus-mediated deletion of NFIA from SVZ progenitor cells
591 *NFIA$^{f/f}$;Rosa-Flox-TdTom* or *NFIA$^{f/+}$;Rosa-Flox-TdTom* mice were bilaterally injected into
592 the subventricular zone, from Bregma: AP= +0.40, DV= −3.40, -3.20, -3.00, -2.80, -2.60,
593 -2.40, ML= −1.00 with 119nl per site of injection along the DV axis. In total, each
594 hemisphere was injected 6 times with 119nl per DV site per hemisphere using Ad5-iCre-
595 GFP virus. All animal procedures were done in accordance with approved BCM IACUC
596 protocols.
597
598 *Human WMI acquisition and staining*
599 All human tissue was collected in accordance with guidelines established by Baylor
600 College of Medicine (H35483). Adult brain MS tissue was acquired through
601 collaboration with the Rocky Mountain Multiple Sclerosis Society. Attainment of
602 neonatal tissue and its hypoxic ischemic encephalopathy (HIE) pathological diagnosis
603 was performed by Dr. Carrie Mohila of Texas Children's Hospital as previously
604 described. IHC on paraffin tissue was performed as previously described (11). Briefly,
605 after deparaffinization, tissue was subjected to antigen retrieval for 7 min in 1x Na
606 citrate, pH 6.0, followed by 15 min of 3% H_2O_2 incubation, blocking, and finally primary
607 antibody incubation overnight. The following antibodies were used: α-NFIA (rabbit,
608 Sigma-Aldrich), α-GFAP (mouse, Millipore). For colorimetric GFAP staining, slides were
609 washed with PBS and then incubated with ImmPRESS HRP α-mouse antibody.
610 Colorimetric reaction was done using ImmPACT DAB peroxidase as per manufacturer
611 guidelines (Vector Laboratories). For double immunolabeling with NFIA on this tissue,
612 following colorimetric DAB peroxidase reaction, slides were washed and then incubated

613 with α-NFIA antibody for 48 hours. NFIA staining was then visualized with goat α-mouse
614 Alexa Fluor 568 (Invitrogen). Slides were counterstained with DAPI and mounted in
615 Vectashield. Slides were then imaged using combined bright field and fluorescent
616 microscopy.
617
618 *Luciferase reporter assay*
619 Mouse Thbs4 promoter (-1 to -810 relative to the transcription start site) containing the
620 putative NFIA binding site was amplified by PCR using mouse genomic DNA, and
621 cloned into pGL3-basic luciferase reporter plasmid (Promega). The putative NFIA
622 binding site was predicted by sequence conservation between species and contains the
623 sequence as follows: 5'-…caaatgggGGATCCTGGCCAaggggcc…-3'.
624 P19 cell line was co-transfected with Thbs4 pGL3-reporter construct, CMV-β-
625 galactosidase vector, and different amounts of pcDNA3-Flag-NFIA using
626 Lipofectamine® 2000 transfection reagent (Thermo-Fisher Scientific). β-galactosidase
627 was used for normalization of transfection efficiency. Cells were harvested 48 hrs post-
628 transfection and luciferase activities were measured using luciferase assay reagent II
629 (LARII) (Promega).
630
631 *In vitro BBB assay and transendothelial electrical resistance measurements*
632 Astrocytes were obtained from the cortices of P0-P1 *NFIA*$^{fl/+}$*; GFAP-CreER* or *NFIA*$^{fl/fl}$*;*
633 *GFAP-CreER* mice using procedures previously described (25,53). Following an
634 additional 7 days of culturing, astrocytes were seeded on opposing sides of trans-well
635 inserts (0.4 um pore size, 12-well; Corning) using methods previously described (25,53).

636 Briefly, astrocytes were seeded on the abluminal side of the poly-d-lysine coated insert
637 at a density of $3x10^4$ cells per filter and allowed to adhere for 2 hours before being
638 inverted back into DMEM F12 containing 10% FBS and 1% PS media. After allowing
639 the astrocytes to grow for 48 hours, the inserts were plated with immortalized mouse
640 endothelial bEnd3 cells (American Type Culture Collection) at a density of $6.6x10^4$ per
641 filter. Transendothelial electrical resistance (TEER) measurements were then made 24
642 hours after bEnd3 seeding using an EVOM resistance meter (World Precision
643 Instruments, Inc.) using Stx2 electrodes. TEER resistance was measured in ohms and
644 normalized to total DAPI+ nuclei on the abluminal side of the membrane (astrocytes)
645 after subtracting resistance from blank trans-well inserts.
646
647 *Evans blue quantification*
648 Evans blue was quantified as previously described in (54). Briefly, 3-month-old mice
649 were injected with a filtered 2% Evans blue solution in PBS by intraperitoneal injection
650 (150 ul/10 g of body weight). Twenty-four hours later, mice were perfused with 1XPBS,
651 and spinal cords or cortices were harvested, weighed, and incubated with 500 ul of
652 formamide for 24 h at 65°C. Subsequently, samples were centrifuged for 30 min at
653 13,200 rpm and absorbance was read at 600 nm. In parallel, a standard curve of Evans
654 blue was performed to calculate the amount of Evans in ng/ul/mg of tissue
655
656 *Chromatin immunoprecipitation (ChIP)*
657 Primary cultures of astrocytes from mouse cortex of postnatal ages (P1-P3) were used
658 for ChIP assays. Harvested cells were washed with PBS buffer and crosslinked with

659 freshly prepared 1% formaldehyde for 10 min at room temperature with rocking. After
660 washing with PBS (containing 1 mM PMSF), the cells were collected by scraping. The
661 cell pellets were further washed with PBS, buffer 1 (10 mM EDTA, 0.5 mM EGTA,
662 0.25% Triton X-100, 10 mM HEPES pH 6.5) and buffer 2 (200 mM NaCl, 1 mM EDTA,
663 0.5 mM EGTA, 10 mM HEPES pH 6.5). The pellets were frozen at -80°C at this stage or
664 resuspended in lysis buffer (0.5% SDS, 5 mM EDTA, 25 mM Tris pH 8, Roche protease
665 inhibitor cocktail). The suspension was sonicated at 4°C in a Branson Sonifier 450. The
666 supernatant was collected and diluted 5-fold with dilution buffer (20 mM Tris pH 8, 150
667 mM NaCl, 2 mM EDTA, 1% Triton X-100, Roche protease inhibitor cocktail), followed by
668 a pre-clearing step mouse IgG (Santa Cruz, sc-2025) and Protein A beads (Invitrogen),
669 at 4°C for 1 hour with shaking. After centrifugation to collect the cell lysate, NFIA
670 antibody (in-house preparation, 10 ug) and rabbit IgG (Santa Cruz, sc-2027) was added
671 to separate immunoprecipitation tubes, at 4°C overnight with shaking. Further
672 incubation with Protein A beads at 4°C for 6 hours was done, followed by collecting the
673 beads and washing the beads four times, 5 minutes each at room temperature with
674 shaking, with cold TSE1 buffer (0.1% SDS, 1% Triton X-100, 2 mM EDTA, 150 mM
675 NaCl, 20 mM Tris pH 8), cold TSE2 buffer (0.1% SDS, 1% Triton X-100, 2 mM EDTA,
676 500 mM NaCl, 20 mM Tris pH 8), LiCl buffer (0.25M LiCl, 1% NP-40, 1% Na
677 deoxycholate, 1 mM EDTA, 10 mM Tris pH 8) and TE buffer (10 mM Tris pH 8, 1 mM
678 EDTA). TE buffer wash was repeated twice and elution buffer (1% SDS, 0.1 M
679 NaHCO3) was added to the beads, vortexed followed by rocking at room temperature
680 for 10 min. The elution was repeated, and supernatant collected and incubated at 65°C
681 overnight, followed by a 2-hour incubation at 42°C with Proteinase K (Promega, 0.05

682 mg/ml). Genomic fragments were purified with phenol/chloroform extraction and DNA
683 pellet was resuspended in water. The ChIP DNA was analyzed by PCR using primers
684 specific to Thbs4 promoter (Forward: 5'-cacctcattccattccgtct; Reverse: 5'-
685 ccgcgctttatggtccag).
686
687
688
689
690 *Imaging of fluorescent and colorimetric staining*
691 Imaging was performed using Zeiss Imager M2 and Z1 fluorescence microscope
692 equipped with a Zeiss AxioCam camera. Analysis was performed using AxioVision and
693 ImageJ software. P values were determined using two-tailed Student's t-test.
694
695 *Statistical analysis*
696 One-way ANOVA was used to analyze the expression of markers to determine the
697 differences between group means, followed by Tukey's test to compare individual
698 means, and it is reported as asterisks in the associated figure graphs. All statistical tests
699 were two-sided. No statistical methods were used to pre-determine sample sizes, but
700 our sample sizes were similar to those reported in previous publications. Data distribu-
701 tion was assumed to be normal, but this was not formally tested. Randomization of
702 animal studies was used in the data analysis. Data collection and analysis were not
703 performed in a blinded manner to the conditions of the experiments. No animal or data
704 points were excluded from the analyses. P-values >0.05 were considered significant.

705

706 *Study Approval*

707 All mouse experiments were approved by the Institutional Animal Care and Use
708 Committee at Baylor College of Medicine and conform to the US Public Health Service
709 Policy on Human Care and Use of Laboratory Animals. Human HIE tissue was collected
710 in accordance with guidelines established by Baylor College of Medicine (H35483).
711 Adult brain MS tissue and normal brain tissue was acquired through collaboration with
712 the Rocky Mountain Multiple Sclerosis Society

713

714 **Author Contributions**

715 DL, TWH, HKL, CTK, and BD conceived the project and designed the experiments; DL,
716 TWH, NABH, YSH, DS, JO, JC, and HKL performed the experiments; CAM, CTK, BRA,
717 SG provided essential reagents; CAM performed all histopathological analyses; DL and
718 BD wrote the manuscript.
719 DL and TWH are listed as co-first authors based on equitable contributions to this
720 manuscript.

721

722 **Acknowledgments**

723 This work was supported by grants from the National Multiple Sclerosis Society (RG-
724 1501-02756 to B.D. and FG-1607-25417 to T.H.), National Institutes of Health
725 (NS096096 to BD and CTK; and NS071153 to B.D.), NIH-NHLBI (T32-HL902332 to
726 DL). Human multiple sclerosis tissue was provided by the tissue bank at the Rocky
727 Mountain MS Center at University of Colorado.

728

729 **References**

730

731 1. Sofroniew MV, Vinters HV. Astrocytes: biology and pathology. Acta Neuropathol.
732 2009;119(1):7-35.
733 2. Renault-Mihara F, Okada S, Shibata S, et al. Spinal cord injury: emerging
734 beneficial role of reactive astrocytes' migration. *Int J Biochem Cell Biol*.
735 2008;40(9):1649-53.
736 3. Voskuhl RR, Peterson RS, Song B, et al. Reactive astrocytes form scar-like
737 perivascular barriers to leukocytes during adaptive immune inflammation of the
738 CNS. *J Neurosci*. 2009;29(37):11511-22.
739 4. Liddelow SA, Guttenplan KA, Clarke LE, et al. Neurotoxic reactive astrocytes are
740 induced by activated microglia. *Nature*. 2017;541(7638):481-487.
741 5. Silver J, Miller JH. Regeneration beyond the glial scar. *Nat Rev Neurosci.*
742 2004;5(2):146-56.
743 6. Pekny M, Pekna M. Astrocyte reactivity and reactive astrogliosis: costs and
744 benefits. Physiol Rev. 2014;94(4):1077-98. doi:10.1152/physrev.00041.2013.
745 7. Liddelow SA, Barres BA. Reactive astrocytes: production, function, and
746 therapeutic potential. *Immunity*. 2017;46(6):957-67.
747 8. Lin CCJ, Yu K, Hatcher A, et al. Identification of diverse astrocyte populations
748 and their malignant analogs. *Nat Neurosci*. 2017;20(3):396-405.
749 9. Sofroniew MV. Molecular dissection of reactive gliosis and glial scar formation.
750 *Trends Neurosci.* 2009;32(12):638-47.

751 10. Anderson MA, Ao Y, Sofroniew MV. Heterogeneity of reactive astrocytes.
752 *Neurosci Lett*. 2013;565:23-9.
753 11. Chaboub LS, Manalo JM, Lee HK, et al. Temporal Profiling of Astrocyte
754 Precursors Reveals Parallel Roles for Asef during Development and after Injury.
755 *J Neurosci*. 2016;36(47):11904-11917.
756 12. Herrmann JE, Imura T, Song B, et al. STAT3 is a critical regulator of astrogliosis
757 and scar formation after spinal cord injury. J Neurosci. 2008;28(28):7231-43.
758 13. Nobuta H, Ghiani CA, Paez PM, et al. STAT3-mediated astrogliosis protects
759 myelin development in neonatal brain injury. *Ann Neurol*. 2012;72(5):750-65.
760 14. Deneen B, Ho R, Lukaszewicz A, et al. The transcription factor NFIA controls the
761 onset of gliogenesis in the developing spinal cord. *Neuron*. 2006;52(6):953-68.
762 15. Kang P, Lee HK, Glasgow SM, et al. Sox9 and NFIA coordinate a transcriptional
763 regulatory cascade during the initiation of gliogenesis. *Neuron*. 2012;74(1):79
764 16. Glasgow SM, Zhu W, Stolt CC, et al. Mutual antagonism between Sox10 and
765 NFIA regulates diversification of glial lineages and glioma subtypes. *Nat*
766 *Neurosci*. 2014;17(10):1322-9.
767 17. Glasgow SM, Carlson JC, Zhu W, et al. Glia-specific enhancers and chromatin
768 structure regulate NFIA expression and glioma tumorigenesis. *Nat Neurosci*.
769 2017;20(11):1520-1528.
770 18. Fancy SP, Glasgow SM, Finley M, Rowitch DH, Deneen B. Evidence that nuclear
771 factor IA inhibits repair after white matter injury. *Ann Neurol*. 2012;72(2):224-33.

772 19. Benner EJ, Luciano D, Jo R, et al. Protective astrogenesis from the SVZ niche
773 after injury is controlled by Notch modulator Thbs4. *Nature*. 2013;497(7449):369-
774 73.
775 20. Labat-gest V, Tomasi S. Photothrombotic ischemia: a minimally invasive and
776 reproducible photochemical cortical lesion model for mouse stroke studies. *J Vis*
777 *Exp*. 2013;(76):50370. Published 2013 Jun 9. doi:10.3791/50370
778 21. Harrington EP, Zhao C, Fancy SP, Kaing S, Franklin RJ, Rowitch DH.
779 Oligodendrocyte PTEN is required for myelin and axonal integrity, not
780 remyelination. *Ann Neurol*. 2010;68(5):703-16.
781 22. Fancy SP, Harrington EP, Yuen TJ, et al. Axin2 as regulatory and therapeutic
782 target in newborn brain injury and remyelination. *Nat Neurosci*. 2011;14(8):1009-
783 16. Published 2011 Jun 26. doi:10.1038/nn.2855
784 23. Kremer D, Aktas O, Hartung HP, Küry P. The complex world of oligodendroglial
785 differentiation inhibitors. Ann Neurol. 2011;69:602–618. doi: 10.1002/ana.22415.
786 24. Obermeier B, Daneman R, Ransohoff RM. Development, maintenance and
787 disruption of the blood-brain barrier. *Nat Med*. 2013;19(12):1584-96.
788 25. Li G, Simon MJ, Cancel LM, et al. Permeability of endothelial and astrocyte
789 cocultures: in vitro blood-brain barrier models for drug delivery studies. *Ann*
790 *Biomed Eng*. 2010;38(8):2499-511.
791 26. Sun W, Cornwall A, Li J, et al. SOX9 Is an Astrocyte-Specific Nuclear Marker in
792 the Adult Brain Outside the Neurogenic Regions. *J Neurosci*. 2017 Apr
793 26;37(17):4493-4507

794 27. Rankin KA, Mei F, Kim K, et al. Selective Estrogen Receptor Modulators
795 Enhance CNS Remyelination Independent of Estrogen Receptors.
796 *J Neurosci*. 2019 Mar 20;39(12):2184-219
797 28. Faiz M, Sachewsky N, Gascón S, et al. Adult neural stem cells from the
798 subventricular zone give rise to reactive astrocytes in the cortex after stroke. *Cell*
799 *Stem Cell*. 2015;17(5):624-34.
800 29. Sun Y, Nadal-Vicens M, Misono S, et al. Neurogenin promotes neurogenesis and
801 inhibits glial differentiation by independent mechanisms. *Cell.* 2001;104(3):365-
802 376.
803 30. He F, Ge W, Martinowich K, et al. A positive autoregulatory loop of Jak-STAT
804 signaling controls the onset of astrogliogenesis. *Nat Neurosci*. 2005;8(5):616-25.
805 31. Koblar SA, Turnley AM, Classon BJ, et al. Neural precursor differentiation into
806 astrocytes requires signaling through the leukemia inhibitory factor receptor. *Proc*
807 *Natl Acad Sci U S A*. 1998;95(6):3178-81.
808 32. Hong S, Song MR. STAT3 but not STAT1 is required for astrocyte differentiation.
809 *PLoS One*. 2014;9(1):e86851. Published 2014 Jan 23.
810 doi:10.1371/journal.pone.0086851.
811 33. Lütolf S, Radtke F, Aguet M, et al. Notch1 is required for neuronal and glial
812 differentiation in the cerebellum. *Development*. 2002;129(2)373-85.
813 34. Shimada IS, Borders A, Aronshtam A, Spees JL. Proliferating reactive astrocytes
814 are regulated by Notch-1 in the peri-infarct area after stroke. *Stroke*.
815 2011;42(11):3231-7.

816 35. Hammond TR, Gadea A, Dupree J, et al. Astrocyte-derived endothelin-1 inhibits
817 remyelination through notch activation. *Neuron*. 2014;81(3):588-602.
818 36. Namihira M, Kohyama J, Semi K, et al. Committed neuronal precursors confer
819 astrocytic potential on residual neural precursor cells. *Dev Cell.* 2009;16(2):245-
820 37. Burda JE, Sofroniew MV. Reactive gliosis and the multicellular response to CNS
821 damage and disease. *Neuron*. 2014;81(2):229-48.
822 38. Eddleston M, Mucke L. Molecular profile of reactive astrocytes – implications for
823 their role in neurologic disease. *Neuroscience.* 1993;54(1):15-36.
824 39. Daginakatte GC, Gadzinski A, Emnet RJ, et al. Expression profiling identifies a
825 molecular signature of reactive astrocytes stimulated by cyclic AMP or
826 proinflammatory cytokines. *Exp Neurol*. 2008;210(1):261-67.
827 40. Yeh T, Lee DY, Gianino SM, Gutmann DH. Microarray analyses reveal regional
828 astrocyte heterogeneity with implications for neurofibromatosis type 1 (NF1)-
829 regulated glial proliferation. *Glia*. 2009;57(11):1239-49.
830 41. Chai H, Diaz-Castro B, Shigetomi E, et al. Neural Circuit-Specialized Astrocytes:
831 Transcriptomic, Proteomic, Morphological, and Functional Evidence. *Neuron*.
832 2017;95(3):531-549.e9.
833 42. Morel L, Chiang MSR, Higashimori H, et al. Molecular and Functional Properties
834 of Regional Astrocytes in the Adult Brain. *J Neurosci*. 2017;37(36):8706-8717.
835 43. Molofsky AV, Kelley KW, Tsai HH, et al. Astrocyte-encoded positional cues
836 maintain sensorimotor circuit integrity. *Nature*. 2014;509(7499):189-94.
837 44. Tsai HH, Li H, Fuentealba LC, et al. Regional astrocyte allocation regulates CNS
838 synaptogenesis and repair. *Science*. 2012;337(6092):358-62.

839 45. Hochstim C, Deneen B, Lukaszewicz A, Zhou Q, Anderson DJ. Identification of
840 positionally distinct astrocyte subtypes whose identities are specified by a
841 homeodomain code. *Cell*. 2008;133(3):510-22.
842 46. Rowitch DH, Kriegstein AR. Developmental genetics of vertebrate glial-cell
843 specification. *Nature*. 2010;468(7321):214-22.
844 47. Burrows RC, Wancio D, Levitt P, Lillien L. Response diversity and the timing of
845 progenitor cell maturation are regulated by developmental changes in EGFR
846 expression in the cortex. *Neuron*. 1997;19(2):251-67.
847 48. Aguirre A, Gallo V. Postnatal neurogenesis and gliogenesis in the olfactory bulb
848 from NG2-expressing progenitors of the subventricular zone. J Neurosci.
849 2004;24(46):10530-41.
850 49. Aguirre A, Dupree JL, Mangin JM, et al. A functional role for EGFR signaling in
851 myelination and remyelination. Nat Neurosci. 2007;10(8):990-1002.
852 50. Glasgow SM, Laug D, Brawley VS, et al. The miR-223/nuclear factor I-A axis
853 regulates glial precursor proliferation and tumorigenesis in the CNS. *J Neurosci*.
854 2013;33(33):13560-8.
855 51. Buffo A, Rite I, Tripathi P, et al. Origin and progeny of reactive gliosis: A source
856 of multipotent cells in the injured brain. *Proc Natl Acad Sci U S A*.
857 2008;105(9):3581-6.
858 52. Lein ES, Hawrylycz MJ, Ao N, et al. Genome-wide atlas of gene expression in
859 the adult mouse brain. *Nature*. 2007;445(7124):168-76.

53. Helms HC, Abbott NJ, Burek M, e. In vitro models of the blood-brain barrier: An overview of commonly used brain endothelial cell culture models and guidelines for their use.t al *J Cereb Blood Flow Metab.* 2016 May;36(5):862-90

54. Menezes MJ, McClenahan FK, Leiton CV, et al. 2014 The extracellular matrix protein laminin_2 regulates the maturation and function of the blood– brain barrier. J Neurosci 34:15260–15280.

883 **Figures**

884

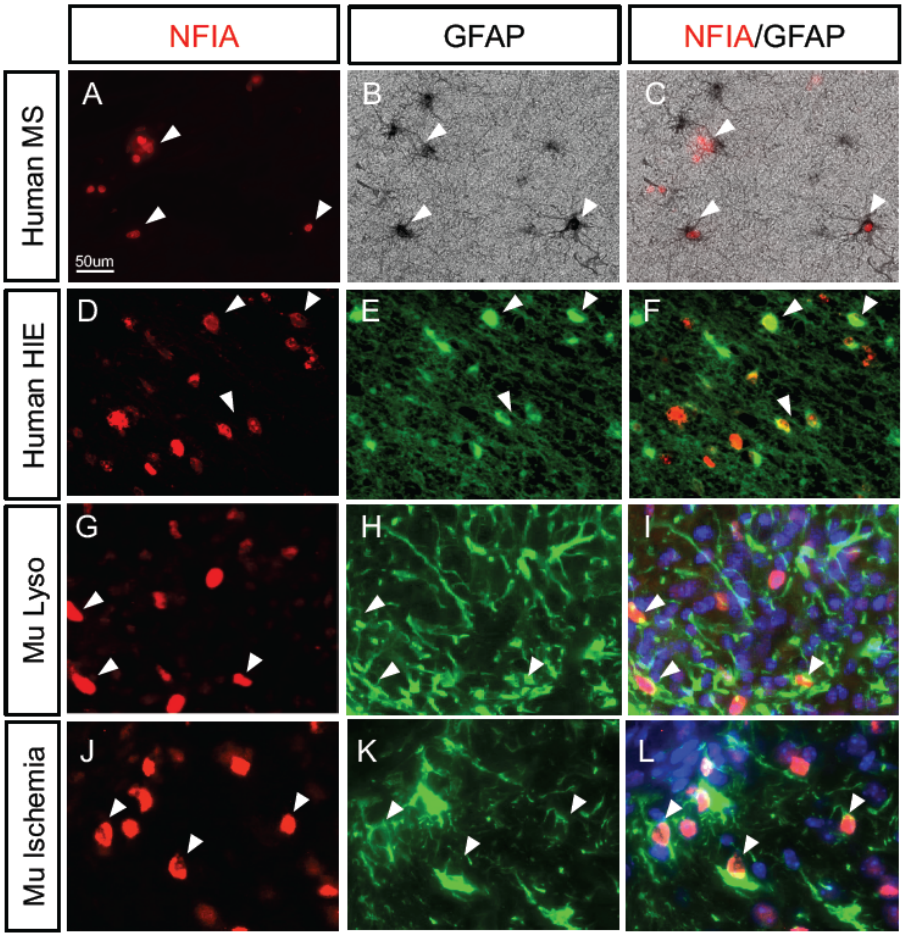

885

886 **<u>Figure 1. NFIA is expressed in reactive astrocytes</u>**. (A-L) Immunofluorescence
887 staining for NFIA and immunohistochemistry staining for GFAP in human MS lesion (A-
888 C), human HIE tissue (D-F), a mouse lysolecithin-induced WM lesion (G-I), and in a
889 mouse photothrombotic ischemia model (J-L). Arrows denote co-localization of NFIA
890 with GFAP in a given image. Images of human tissue samples in A-F are representative
891 of 3 patients and 8 sections per patient. Images of tissue from mouse models in G-L are
892 representative of per 5 animals and 8 sections per animal. Representative scale bar in
893 A is 50um.

894

895

896

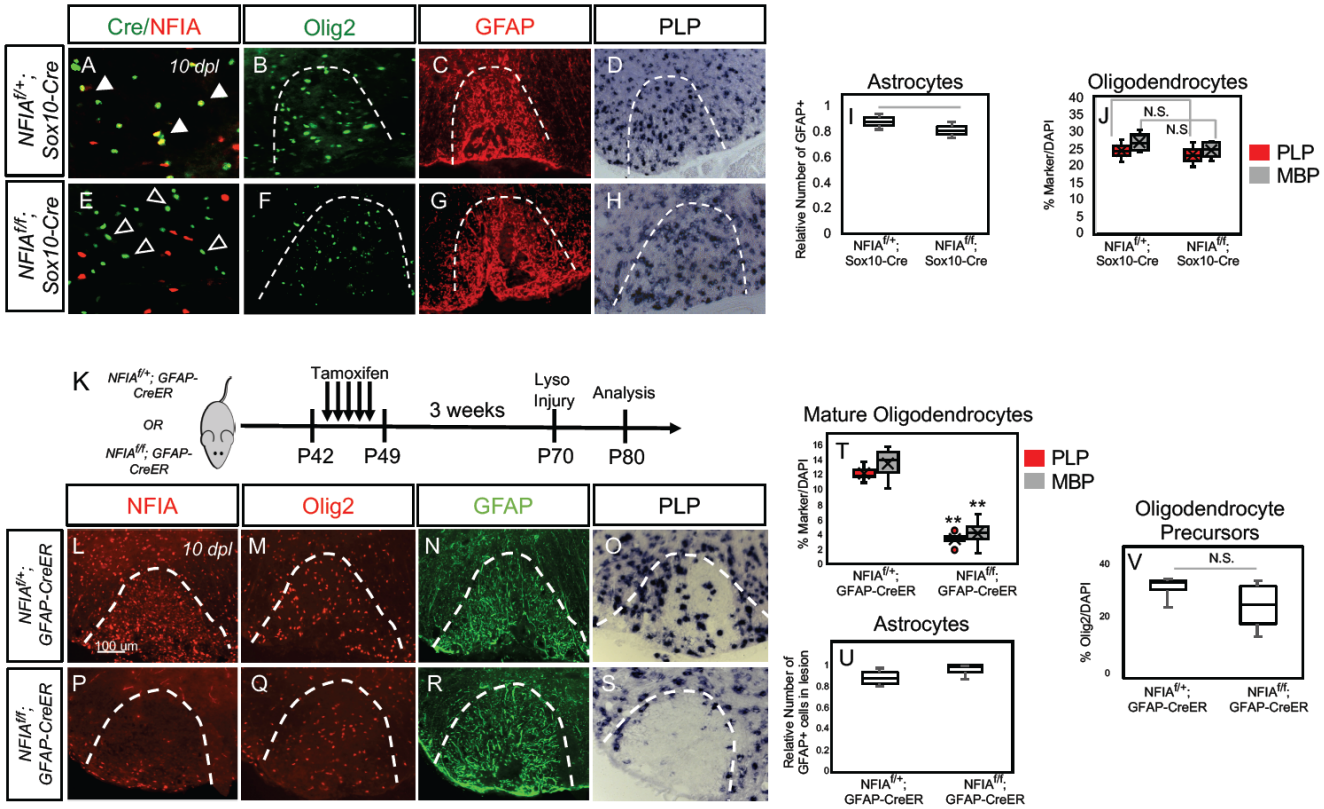

897

898 **<u>Figure 2. Loss of NFIA from astrocytes delays oligodendrocyte differentiation</u>**

899 **<u>after WMI.</u>** (A-H) Loss of NFIA from oligodendrocyte lineage does not affect the number

900 of Olig2-expressing cells (B, F), GFAP-expressing cells (B, G, I), or PLP-expressing

901 cells (D-H, J) within the lesion after injury at 10dpl. Filled arrows in A denote

902 Sox10/NFIA co-expressing OLP populations, open arrows in E denote Sox10-positive

903 cells that do not express NFIA in *NFIA$^{f/f}$; Sox10-Cre* mice. (K) Schematic overview of

904

905 GFAP-CreERT2 induction schedule and subsequent WMI time course. (L-S) Induced

906 deletion of NFIA in *NFIA$^{f/f}$; GFAP-CreER* mice effectively eliminates NFIA expression in

907 the lesion (L v. P) and does not affect the number of Olig2- or GFAP-expressing cells
908 within the lesion (Q-R), but results decreased PLP-expressing cells within the injury site
909 (S). Dashed lines in A-H and L-S indicate lesion boundary. (R-S) Quantification of
910 reactive astrocytes (GFAP) and OL marker expression (MBP and PLP) in astrocyte-
911 specific NFIA-knockout studies. For the analysis in I-J and T-V, experiments were
912 performed on four animals per genotype, and quantification involved eight sections per
913 animal. Data were analyzed by Student's *t* test. Data are shown by box and whisker
914 plots. The bounds of the boxes represent upper and lower quartiles. The lines in the
915 boxes represent the median, and the whiskers represent the maximum and minimal
916 values.. PLP **p=1.87E-9; MBP **p=9.32E-6. See supplemental data for MBP in situ
917 hybridization. Representative scale bar is 100um.
918
919
920
921
922
923
924
925
926
927

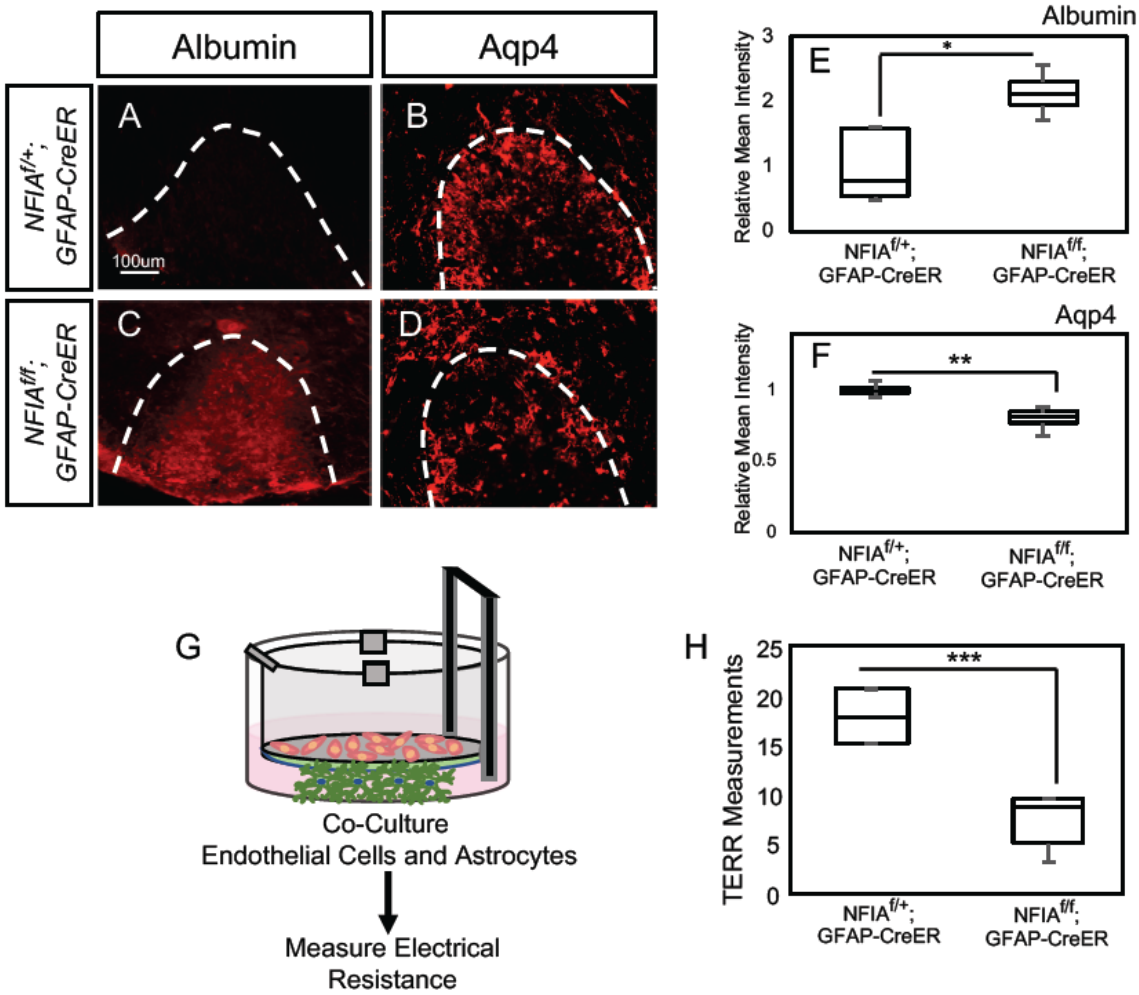

928

929 **Figure 3. NFIA-deficient astrocytes exhibit impaired BBB remodeling after WMI.**

930 (A-D) Deletion of NFIA from astrocytes results in an increase in the presence of Albumin

931 (A v. C) and decrease in the expression of astrocyte endfeet protein Aqp4 (B v. D.)

932 Graphs in E-F are derived from four animals per genotype, and quantification involved

933 eight sections per animal. (G) Schematic overview of in vitro endothelial/astrocyte

934 barrier assay. (H) NFIA-deficient astrocytes exhibit decreased TEER electrical

935 resistance when co-cultured with endothelial cells. Experiment was conducted in

936 triplicate with 3 co-culture wells per genotype for each replicate. Data were analyzed by

937 Student's *t* test. Data are shown by box and whisker plots. The bounds of the boxes

938 represent upper and lower quartiles. The lines in the boxes represent the median, and
939 the whiskers represent the maximum and minimal values. *p=0.01, **p=0.003,
940 ***p=0.0036. Representative scale bar is 100um.
941
942
943
944
945
946
947
948
949
950
951
952
953
954
955
956
957
958
959
960

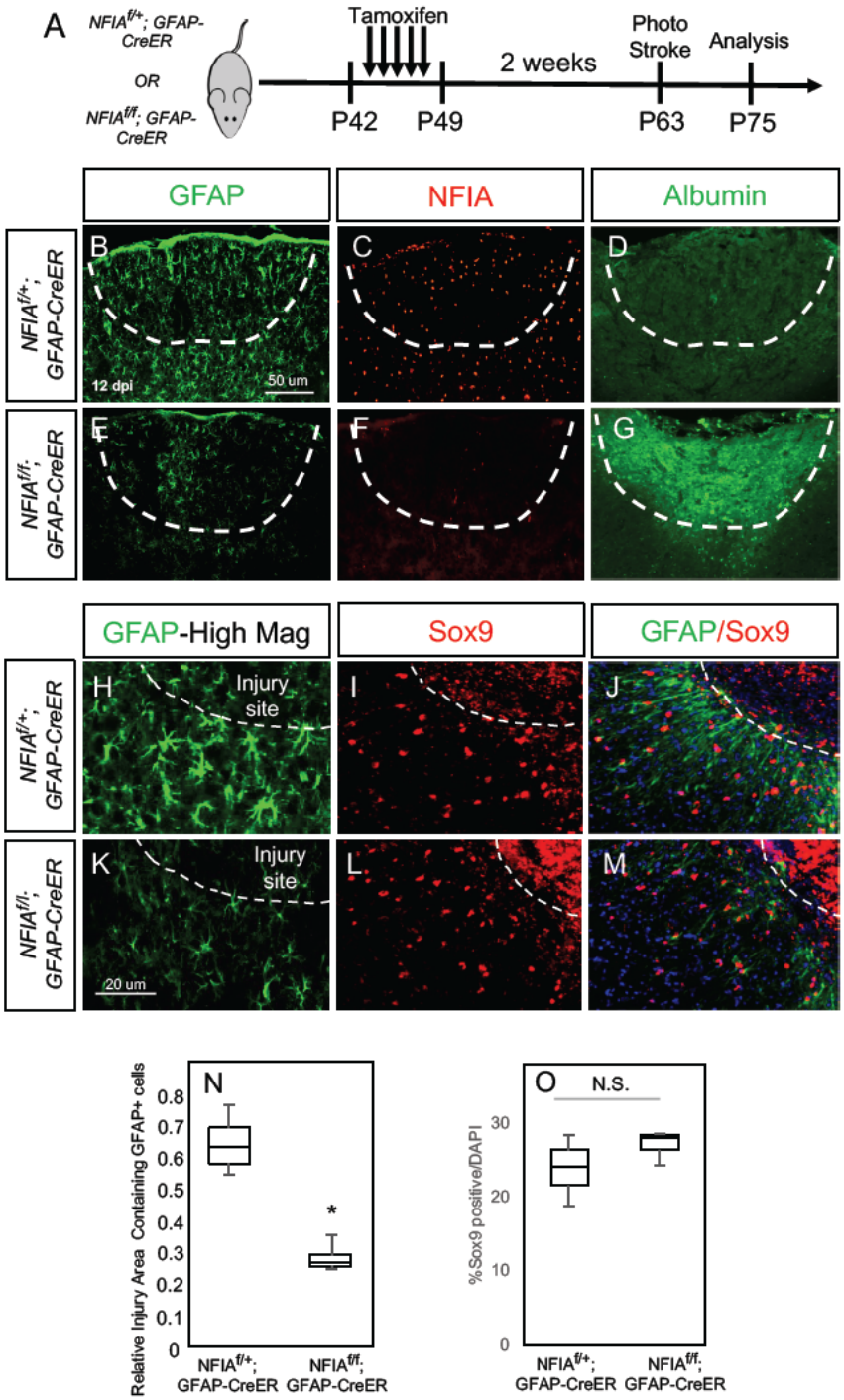

961

962 **<u>Figure 4. NFIA is required for the generation of reactive astrocytes after ischemic</u>**

963 **<u>stroke.</u>** (A) Overview of experimental procedure for GFAP-CreER induction and stroke

964 injury model. (B-G) Loss of NFIA in astrocytes results in reduction of GFAP+ reactive

965 astrocytes (B v. E) and an increase in blood serum protein Albumin (D v. G) at stroke
966 injury site at 12dpi. Dashed lines in B-I indicate injury boundary. (H-M) High
967 magnification images of GFAP+ and Sox9+ cells at the injury site in control and *NFIA*$^{f/f}$*;*
968 *GFAP-CreER* mice, indicating a decrease in the number of GFAP+ reactive astrocytes
969 at the injury site, coupled with no change in the number of Sox9+ cells. Quantification of
970 GFAP+ reactive astrocytes (N) or Sox9-expressing cells (O) in response to
971 photothrombotic stroke model in control and *NFIA*$^{f/f}$*; GFAP-CreER* mice. Quantification
972 derived from 4 animals for (N) and 3 animals for (O) per genotype and 8 sections per
973 animal. Data were analyzed by Student's *t* test. Data are shown by box and whisker
974 plots. The bounds of the boxes represent upper and lower quartiles. The lines in the
975 boxes represent the median, and the whiskers represent the maximum and minimal
976 values. *p=0.0092. Representative scale bar in B is 50um and scale bar in K is 20um.
977
978
979
980
981
982
983
984
985
986
987

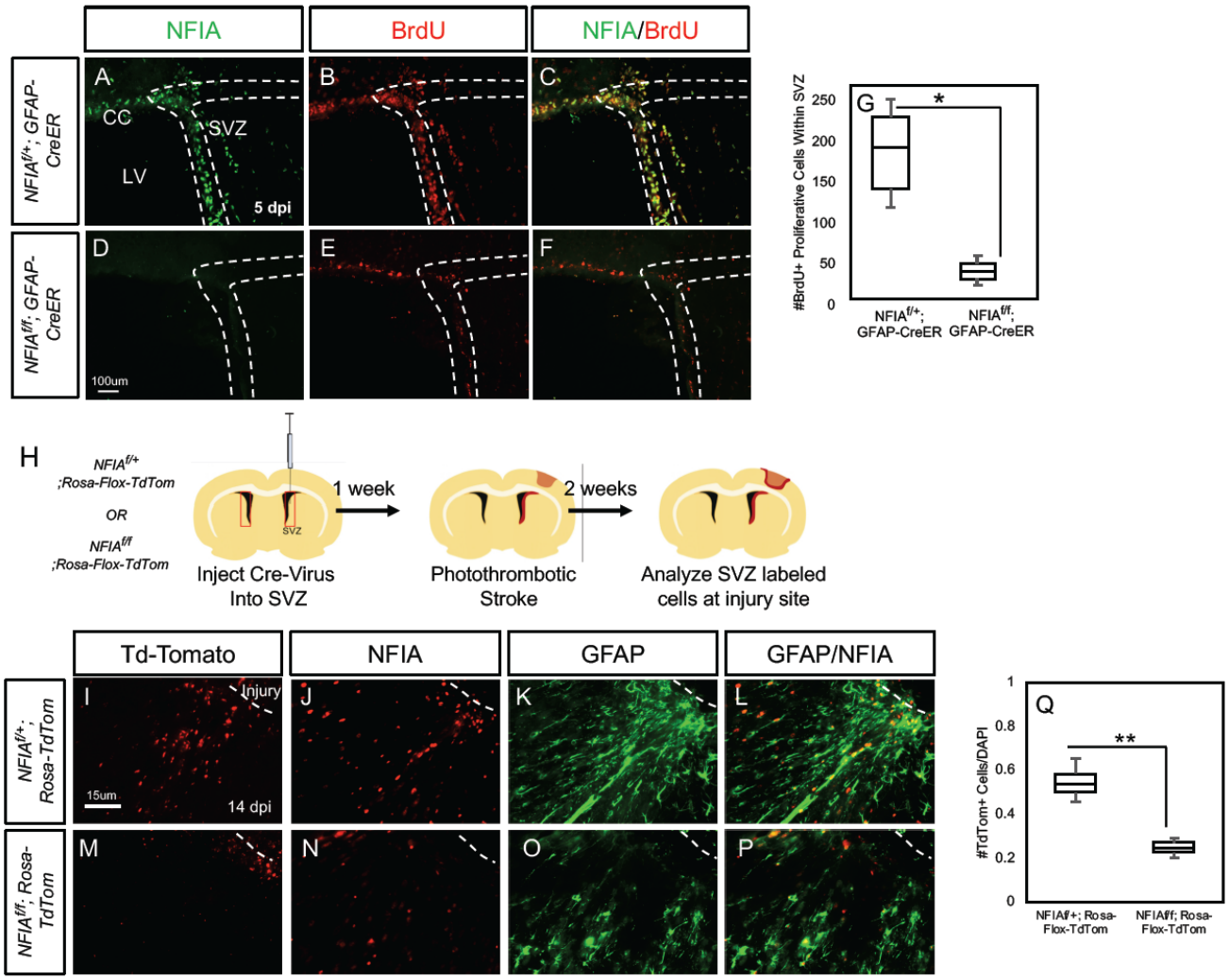

Figure 5. Selective deletion of NFIA in the SVZ impairs reactive astrocyte production after ischemia. (A-C) NFIA is expressed in proliferating, BrdU+ populations in the SVZ at 5dpi and genetic deletion of NFIA with *GFAP-CreER* results in decreased proliferation, measured by BrdU incorporation in SVZ populations (D-F). (G) Quantification of BrdU+ cells within the SVZ after injury in control and *NFIA$^{f/f}$; GFAP-CreER* mice. Quantification derived from 5 control and 4 experimental animals and 8 sections per animal, *p=0.0016. (H) Experimental timeline for Cre-Virus mediated deletion of NFIA from SVZ progenitor cells and subsequent photothrombotic stroke and analysis. (I-L) Control experiments showing SVZ-derived, TdTomato-labeled

998 populations (I), express NFIA (J), and generate reactive astrocytes that reside at the
999 injury site (K-L). (M-P) Deletion of NFIA from SVZ populations results in decreased
1000 number of TdTom+ cells at injury site (M), reduced NFIA (N) and GFAP expression (O-
1001 P) at injury site. (Q) Quantification of TdTom+ cells at injury border in *NFIA*$^{f/+}$*; Rosa-*
1002 *TdTom* and *NFIA*$^{f/f}$*; Rosa-TdTom.* Quantification derived from 8 sections per animal and
1003 3 animals per genotype. Data were analyzed by Student's *t* test. Data are shown by box
1004 and whisker plots. The bounds of the boxes represent upper and lower quartiles. The
1005 lines in the boxes represent the median, and the whiskers represent the maximum and
1006 minimal values. *$p<0.05$, **$p=0.0065$. Representative scale bar in D is 100um and
1007 scale bar in I is 15um.
1008
1009
1010
1011
1012
1013
1014
1015
1016
1017
1018
1019
1020

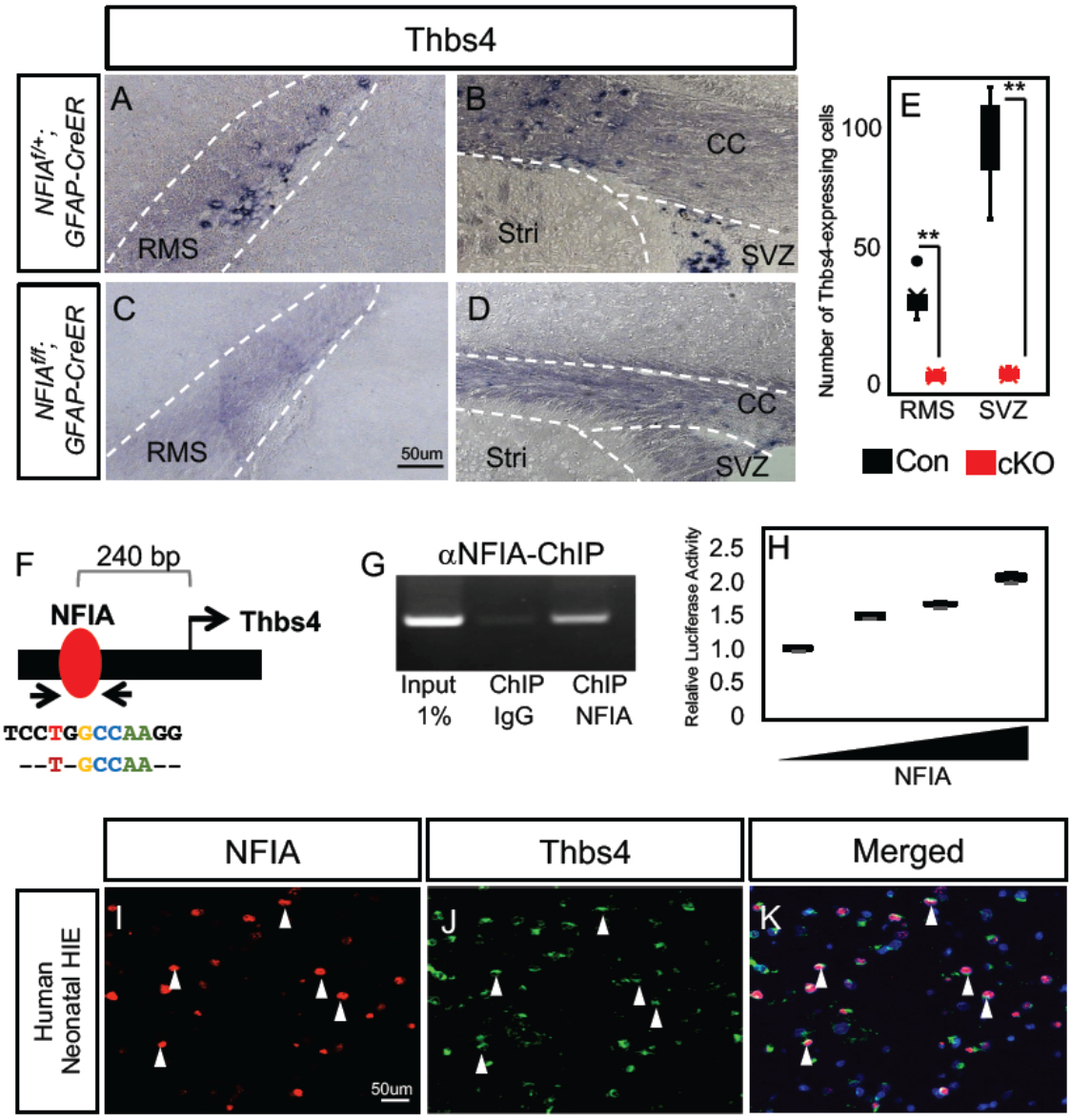

Figure 6. NFIA directly regulates the expression of Thbs4. (A-D) Deletion of NFIA results in decreased Thbs4 mRNA expression within the rostral migratory stream (RMS) and SVZ regions. (E) Quantification of Thbs4 in situ hybridization signal within the RMS and SVZ of *NFIA$^{f/+}$; GFAP-CreER versus NFIA$^{f/f}$; GFAP-CreER mice.* Quantification performed by analyzing 8 sections per animal and 3 mice per genotype. Data were analyzed by Student's *t* test. Data are shown by box and whisker plots. The bounds of the boxes represent upper and lower quartiles. The lines in the boxes represent the

1029 median, and the whiskers represent the maximum and minimal values. RMS
1030 **p=0.000053, SVZ **p=0.0000026 (F) Illustration of the prospective NFIA binding site
1031 240 bp upstream of the Thbs4 transcriptional start site and alignment with consensus
1032 NFIA-binding sequence. (G) Anti-IgG and anti-NFIA antibodies were used to
1033 immunoprecipitated DNA fragments from cultured astrocytes. Fragments were analyzed
1034 via PCR using primers designed to include the prospective NFIA binding site within the
1035 Thbs4 promoter region, showing NFIA binds this predicted site. (H) Increasing
1036 concentrations of NFIA result in an increased activation of a luciferase reporter plasmid
1037 containing the Thbs4 promoter region when co-transfected in P19 cells. Data are shown
1038 by box and whisker plots. The bounds of the boxes represent upper and lower quartiles.
1039 The lines in the boxes represent the median, and the whiskers represent the maximum
1040 and minimal values. (I-K) Fluorescent immunostaining for NFIA combined with
1041 fluorescent in situ hybridization labeling of Thbs4 indicates co-expression within human
1042 neonatal HIE tissue; filled arrows denote co-labeling of Thbs4 and NFIA. Images in I-K
1043 are representative of 3 individual patients, 8 sections per patient. Representative scale
1044 bars in C and I are each 50um.
1045
1046
1047
1048
1049
1050
1051

1052 **Supplemental Figure Legends**

1053

1054 **Supplemental Figure 1. Models of WMI and cortical ischemic stroke.** (A-D)
1055 Illustration of lysolecithin-induced WM lesion injection and stereotypic time course of
1056 oligodendrocyte differentiation following such injury modeling. Dashed line in B-D
1057 indicates injury boundary. (E) Illustration of photothrombotic model of cortical ischemic
1058 stroke.

1059

1060

1061 **Supplemental Figure S2. NFIA is expressed in astrocytes in the adult brain**
1062 (A-C) Co-immunofluorescence staining for NFIA and GFAP in normal adult human
1063 cortex and (D-F) normal mouse cortex. Arrows denote co-localization of NFIA with
1064 GFAP in a given image. Images of human tissue samples in A-C are representative of
1065 3 samples of non-lesioned cortical tissue and 8 sections per patient. Images of tissue
1066 from mouse models in D-F are representative of 5 animals and 8 sections per animal.
1067 Representative scale bar in A is 20um.

1068

1069

1070 **Supplemental Figure 3. Analysis of oligodendrocyte differentiation and axonal**
1071 **integrity in *NFIA$^{fl/fl}$; GFAP-CreER mice* at 10 and 12dpl.** (A-B) Oligodendrocyte
1072 differentiation at 10dpl, as marked by MBP *in situ* hybridization, is delayed in *NFIA$^{f/f}$;*
1073 *GFAP-CreER* mice compared to control *NFIA$^{f/+}$; GFAP-CreER* mice. Images are
1074 representative of four animals per genotype and eight sections per animal. (C-F)

1075 Lesions in the *NFIA*$^{fl/fl}$*; GFAP-CreER* mice contained PLP- and MBP- expressing cells at
1076 12dpl at comparable levels to control *NFIA*$^{fl/+}$*; GFAP-CreER* mice. Images are
1077 representative of 8 sections per animal and 3 animals per genotype. (G-N)
1078 Immunostaining for axonal markers NF200 (H, L) and SMI32 (I,M) in lysolecithin lesions
1079 from *NFIA*$^{f/f}$*; GFAP-CreER* and *NFIA*$^{f/+}$*; GFAP-CreER* mice. Quantification in O and P is
1080 derived from three animals per genotype and eight sections per animal. Data were
1081 analyzed by Student's *t* test, **P*<0.05. Data are shown by box and whisker plots. The
1082 bounds of the boxes represent upper and lower quartiles. The lines in the boxes
1083 represent the median, and the whiskers represent the maximum and minimal values.
1084 Representative scale bar is 50um.
1085
1086
1087 **Supplemental Figure 4. Analysis of oligodendrocyte regeneration after lysolecitin**
1088 **lesioning of the corpus callosum.** (A-F) Analysis of reactive astrocyte responses in
1089 the corpus callosum 12 days post lysolecithin lesioning in *NFIA*$^{f/f}$*; GFAP-CreER* and
1090 *NFIA*$^{f/+}$*; GFAP-CreER* mice revealed no changes in the extent of GFAP (A v. D; G) or
1091 Sox9 (B v. E; H) expression in these lesions. (I-N) Analysis of oligodendrocyte
1092 responses in the corpus callosum revealed no differences in the number of Olig2-
1093 expressiong progenitor populations (I v. K; N) or PLP-expressing differentiated
1094 populations (J v. L; M). Quantification in G-H and M-N is derived from three animals per
1095 genotype and six sections per animal. Data were analyzed by Student's *t* test, **P*<0.05.
1096 Data are shown by box and whisker plots. The bounds of the boxes represent upper

1097 and lower quartiles. The lines in the boxes represent the median, and the whiskers
1098 represent the maximum and minimal values. Representative scale bars are 200um.
1099
1100
1101 **Supplemental Figure 5. TdTomato labeling of SVZ cells after Ad5-Cre injection**
1102 **and photothrombotic stroke.** (A) Analysis of the relative amount of Evans blue
1103 extracted from the spinal cord or cortex from 3-month-old mice. In each case, for each
1104 genetic condition and region, Evans blue was extracted and quantified as ug/ul/mg of
1105 tissue. N=3 for each genetic condition, for both spinal cord and cortex. Data were
1106 analyzed by Student's *t* test, $*P<0.05$. Data are shown by box and whisker plots. The
1107 bounds of the boxes represent upper and lower quartiles. The lines in the boxes
1108 represent the median, and the whiskers represent the maximum and minimal values.
1109 (B-C) Both *NFIA$^{f/f}$; Rosa-TdTom* and *NFIA$^{f/+}$; Rosa-TdTom* mice show TdTom+ cells
1110 within the SVZ, indicating Ad5-Cre infection results in recombination. A large proportion
1111 of TdTom+ cells remain in the SVZ in *NFIA$^{f/f}$; Rosa-TdTom* mice compared to control
1112 *NFIA$^{f/+}$; Rosa-TdTom* mice. Images are representative of 8 sections per animal and 3
1113 animals per genotype. (D-I) BrdU-labeling of *NFIA$^{f/f}$; GFAP-CreER* and *NFIA$^{f/+}$; GFAP-*
1114 *CreER* mice under uninjured conditions, reveals a drastic reduction in BrdU
1115 incorporation in the SVZ in the absence of NFIA (E-F v. H-I). Images are representative
1116 of at least three animals per genotype and at least six sections per animal.
1117 Representative scale bar is 100um.
1118
1119

1120 **Supplemental Figure S6. Thbs4 expression in the SVZ is reduced in the absence**

1121 **of NFIA.** Immunfluorescence staining with Thbs4 and DAPI counterstain in the SVZ of

1122 *NFIA$^{f/f}$; GFAP-CreER* and *NFIA$^{f/+}$; GFAP-CreER* under normal conditions (A,C) and

1123 after ischemic stroke (B,D). Results demonstrate that Thbs4 expression is drastically

1124 reduced under homeostatic and after injury in the absence of NFIA. Images are

1125 representative of three animals per genotype and four sections per animal.